Single and multiple vortex rings in three-dimensional Bose-Einstein condensates: Existence, stability, and dynamics

Wenlong Wang,[1,*] R. N. Bisset,[2] C. Ticknor,[3] R. Carretero-González,[4,‡]
D. J. Frantzeskakis,[5] L. A. Collins,[3] and P. G. Kevrekidis[6,†]
[1]*Department of Physics and Astronomy, Texas A&M University, College Station, Texas 77843-4242, USA*
[2]*INO-CNR BEC Center and Dipartimento di Fisica, Università di Trento, Via Sommarive 14, I-38123 Povo, Italy*
[3]*Theoretical Division, Los Alamos National Laboratory, Los Alamos, New Mexico 87545, USA*
[4]*Nonlinear Dynamical Systems Group, Computational Sciences Research Center, and Department of Mathematics and Statistics, San Diego State University, San Diego, California 92182-7720, USA*
[5]*Department of Physics, National and Kapodistrian University of Athens, Panepistimiopolis, Zografos, Athens 15784, Greece*
[6]*Department of Mathematics and Statistics, University of Massachusetts, Amherst, Massachusetts 01003-4515, USA*
(Received 13 February 2017; published 27 April 2017)

In the present work, we explore the existence, stability, and dynamics of single- and multiple-vortex-ring states that can arise in Bose-Einstein condensates. Earlier works have illustrated the bifurcation of such states in the vicinity of the linear limit for isotropic or anisotropic three-dimensional harmonic traps. Here, we extend these states to the regime of large chemical potentials, the so-called Thomas-Fermi limit, and explore their properties such as equilibrium radii and inter-ring distance for multi-ring states, as well as their vibrational spectra and possible instabilities. In this limit, both the existence and stability characteristics can be partially traced to a particle picture that considers the rings as individual particles oscillating within the trap and interacting pairwise with one another. Finally, we examine some representative instability scenarios of the multi-ring dynamics, including breakup and reconnections, as well as the transient formation of vortex lines.

DOI: 10.1103/PhysRevA.95.043638

I. INTRODUCTION

Bose-Einstein condensates (BECs) of ultracold atomic gases have, for around two decades now [1–4], captured not only the interest of the atomic, molecular, and optical physics communities but also considerably that of the nonlinear wave community [5,6]. This, to a significant degree, is due to the effective nonlinearity introduced at the lowest-order mean-field theory [1,2,6], which leads to a nonlinear Schrödinger-type equation [7–10], referred to as the Gross-Pitaevskii equation (GPE). Depending on the sign of the s-wave scattering length, this results in a self-defocusing or self-focusing nonlinearity in the equation (corresponding to repulsive or attractive interatomic interactions, respectively), which, in turn, admits an array of relevant nonlinear wave structures. The latter comprise, but are not limited to, bright [11–13], gap [14], and dark [15] matter-wave solitons. In higher dimensions and for repulsive interatomic interactions, the main structures are vortices [16,17] in two dimensions and, additionally, vortex lines and rings in three dimensions [18].

Our focus in the present work will be on vortex rings (VRs) arising in three-dimensional (3D) repulsive BECs. Such structures have been studied rather extensively in theoretical, computational, and experimental works, with a number of reviews having emerged from this activity [5,6,18], as well as more general works regarding fluids and superfluids [19–21]. In addition to their much earlier observation in helium [22–24], established techniques for the experimental realization of vortex rings in BECs include the decay of planar dark solitons [25], creation via density engineering [26], spontaneous emergence via the collision of symmetric defects [27], and their detection through unusual collision outcomes of dark solitonic structures [28]. Given their emergence (often in a spontaneous way) through a variety of nonequilibrium situations, vortex rings are of general interest in atomic BECs in 3D geometries [6,18]. At the same time, they play an important role within the theory of quantum turbulence [29–31]. More specifically, vortex-ring stability, their decay pathways, and time scales are of fundamental importance to turbulent processes, such as the redistribution of vorticity among the length scales [32–34], or the conversion of superfluid kinetic energy into sound via the Kelvin-wave cascade [35–37].

In recent years, a program of exploring coherent structures in a two-pronged way has naturally emerged and has been summarized, e.g., in Ref. [6]. On the one hand, it is possible to study nonlinear waves in the vicinity of the linear (noninteracting) limit of the GPE, namely, that of the quantum harmonic oscillator. This limit, while physically less relevant given its association with small atom numbers, is very insightful towards the wave forms that are possible via different combinations of the linear eigenfunctions; incidentally, this regime is also more prone to important quantum-fluctuation phenomena [38]. In the context of VRs and related states, this approach has been utilized, e.g., in Refs. [39,40] to construct single- and multiple-VR structures. On the other hand, a complementary approach that is certainly relevant experimentally is the exploration of the highly nonlinear, large-atom-number regime. This is known as the Thomas-Fermi (TF) limit, in which the structures become narrower as the healing length, which constitutes their characteristic length scale, decreases. Here, the coherent waves can be thought of as individual "particles" that have kinematics and interparticle dynamics that can be approximated by suitable

*wenlongcmp@gmail.com
†kevrekid@math.umass.edu
‡http://nlds.sdsu.edu

particle models. Although attempts have been made to explore a single VR as such a particle, to describe its vibrational modes [41–44], and to explore multiple VRs in a homogeneous (untrapped) medium [19,45–47], to the best of our knowledge no such attempt has been made for the case of multiple trapped VRs. It is the purpose of this work to contribute to this direction by developing a systematic approach to study this problem. We thus show that multiple trapped VRs are especially important: this is due to the fact that the interplay of the intrinsic dynamics of each VR, with the trapping and inter-VR interactions, produces the possibility of stationary multi-VR states that we will argue, based on their stability properties, are experimentally accessible. It is also shown that multiple VRs also produce intriguing vibrational dynamics within both the stable and unstable regimes.

The presentation of the paper is structured as follows. In Sec. II A we outline the numerical formulation of the three-dimensional GPE and its Bogoliubov–de Gennes (BdG) spectral stability analysis. In the theoretical formulation of Sec. II B, we present the "particle picture" (PP) that we will use to provide insights into the single- and multiple-VR steady states. Then, in Sec. III, we discuss our numerical results, first, for the cases of the single and double VRs and, finally, for that of a triple-VR state that we can also systematically construct and probe. We make direct comparisons between the treatments to illustrate the qualitative ability of the theory to capture multi-VR states. Our existence and stability computations, together with the PP analysis, are complemented by a selection of dynamical manifestations of both the vibrational modes, such as those that describe the relative motion of multiple VRs, and the intriguing instabilities in certain regimes. Finally, in Sec. IV, we summarize our findings, discuss some open problems, and present a number of possibilities for future studies.

II. THEORETICAL AND COMPUTATIONAL MODEL SETUP

A. The Gross-Pitaevskii equation

In the framework of the lowest-order mean-field theory, for sufficiently low temperatures, the dynamics of a 3D repulsive BEC is well described by the GPE [1,2,5,6],

$$i\hbar\psi_t = -\frac{\hbar^2}{2m}\nabla^2\psi + V\psi + g|\psi|^2\psi - \mu\psi, \tag{1}$$

where $\psi(x,y,z,t)$ is the macroscopic wave function, μ is the chemical potential, and $g = 4\pi\hbar^2 a_s/m$, with a_s being the s-wave scattering length and m being the atomic mass. We use a harmonic trap of the form

$$V(\vec{r}) = \tfrac{1}{2}m\left(\omega_r^2 r^2 + \omega_z^2 z^2\right), \tag{2}$$

where $r^2 = x^2 + y^2$ and ω_r and ω_z are the trapping frequencies along the radial and axial directions, respectively. Note that the potential has rotational symmetry with respect to the z axis. In our simulations we study the two-VR state with $\omega_z = \omega_r$, while we explore the three-VR state with $\omega_z = \frac{2}{3}\omega_r$. In these settings, the two states have chemical potentials at the linear (noninteracting) limit equal to $\mu_c = \frac{7}{2}\hbar\omega_r$ and $\frac{10}{3}\hbar\omega_r$, respectively. This occurs when the ring-dark-soliton state becomes energetically degenerate with either the two- or three-planar-dark-soliton state, enabling combinations of two states with a relative phase difference of $\pi/2$ that give rise to the two-VR or three-VR states, respectively [39,40]. These states can then be numerically followed all the way from the above-mentioned linear limit to the large-chemical-potential, highly nonlinear limit. We have also performed the corresponding BdG spectral analysis of the states as a function of the chemical potential using the linearization ansatz,

$$\psi(\vec{r},t) = \psi_0(\vec{r}) + \epsilon[a(\vec{r})e^{\lambda t} + b^*(\vec{r})e^{\lambda^* t}]. \tag{3}$$

Here, ψ_0 denotes the single- or multi-VR stationary state whose stability is sought, ϵ is a formal perturbation parameter, and λ denotes the eigenvalue corresponding to the eigenvector $(a,b)^T$, with $(\cdot)^T$ denoting the transpose and $(\cdot)^*$ denoting complex conjugation.

We temporally evolve the GPE, Eq. (1), using two independent methods, providing a strong test of our numerics. In one method, we utilize a real-space product scheme with a finite-element discrete-variable representation. This is based on a split-operator approach, and a Gauss-Legendre quadrature is implemented within each element [48,49]. In the other method, a split-step operator is performed on a fast-Fourier-transform (FFT) grid. Our BdG calculations are made feasible by implementing a Fourier-Hankel scheme that utilizes azimuthal symmetry, much as was done in Refs. [50,51]. In addition to allowing one to treat 3D functions as two-dimensional (2D), numerically, this allows the diagonalization of each angular momentum subspace individually.

In what follows, we are interested in both the properties of the GPE solutions themselves, such as the equilibrium radial or axial positions, and those of their excitations. We will also attempt to connect the GPE solutions with our particle-picture results.

B. The particle picture of vortex rings in a trap

We now focus on the limit of large chemical potentials μ, where we can provide a theoretical analysis of the in-trap dynamics and interactions of multiple VRs. For simplicity, in all that follows we have used dimensionless units (see, e.g., Refs. [5,6]) where time is measured in units of inverse trap frequency ($1/\omega_r$), length scales are in units of harmonic oscillator length ($a_r = \sqrt{\hbar/m\omega_r}$), and energy units are $\hbar\omega_r$. In this TF limit, there exists a well-known approximation to the ground state of the GPE given by $\psi_{\rm TF} = \sqrt{\max[\mu - V(\vec{r}),0]}$. Here, our aim is to explore vortical excitations (in particular, VRs) on top of this ground state. As indicated in the Introduction, studies have independently considered each of the following:(i) the motion of a single VR in a homogeneous setting [52], (ii) the effect of a trap on a single VR [41–43,53], and (iii) the interaction of multiple VRs in the absence of a trap [19,45–47].

Another aim of this work, in addition to exploring the existence, stability, and dynamics of these states, is to explore the effective PP model arising from combining these different ingredients together and its usefulness in capturing the essential static properties corresponding to equilibrium configurations of multiple VRs in a trap as well as the periodic oscillations ensuing from initial conditions away from these equilibria.

For a set of coaxial VRs along the z axis, a naïve approach to combine the above-mentioned VR-VR and VR-trap contributions would consist of simply *adding* the corresponding reduced dynamics at the level of the effective ordinary differential equations (ODEs) on the VR radii r_i and positions z_i. However, perhaps somewhat surprisingly, this approach turns out to produce *non-Hamiltonian* ODEs because the two main contributions, namely, the VR-VR interaction [45] and VR-trap interaction [53], originate from energy terms with *different* canonical variables (see below). Therefore, this approach, although capable of reasonably predicting the positions for stationary multi-VR configuration (results not shown here), fails to describe the actual dynamics of trapped multi-VR configurations. In fact, the ensuing VR dynamics for this naïve approach give rise to orbits that fail to be closed.

In order to derive a self-consistent Hamiltonian set of equations for trapped multi-VR configurations it is necessary to start from the Hamiltonian formulation of the different interaction energies involved and then obtain the equations of motion through a common set of canonical variables. Let us then consider the following energies: (i) the VR-trap energy, denoted by $E_{\text{VR-T}}$, described in Ref. [53] and (ii) the VR-VR energy, denoted by $E_{\text{VR-VR}}$, described in Ref. [45]. Importantly, both $E_{\text{VR-T}}$ and $E_{\text{VR-VR}}$ contain the VR self-induced velocity that is responsible for a single VR to always have an intrinsic velocity. Therefore, we construct the total energy of the system with the following combination that includes the self-induced interaction only once:

$$\begin{aligned} E &= E_{\text{VR-T}} + E_{\text{VR-VR}} - E_{\text{VR-VR}}^{\text{self}} \\ &= E_{\text{VR-T}} + \tilde{E}_{\text{VR-VR}}, \end{aligned} \tag{4}$$

where $E_{\text{VR-VR}}^{\text{self}}$ corresponds to the contribution to the energy originating from the self-induced velocity in the untrapped VR-VR description [45]. Specifically, using Refs. [45,53], to describe these contributions yields the following energies. The VR-T contribution for a single VR at position (r_i,z_i) inside an isotropic ($\omega = \omega_r = \omega_z$) trapping potential with TF radius $R_\perp = \sqrt{2\mu}/\omega$ yields [53]

$$E_{\text{VR-T}} = 2\pi\,\mu\,r_i\left[\left(1-\frac{r_0^2}{R_\perp^2}\right)\ln\left(\frac{\sqrt{R_\perp^2-r_0^2}}{\xi}\right)+\frac{r_0^2}{R_\perp^2}-1\right], \tag{5}$$

with $r_0^2 = r_i^2 + z_i^2$, where $\xi = 1/\sqrt{a\mu}$ is obtained from the $r \approx 0$ asymptotics of the vortex core density $\rho(r) \approx a\mu^2 r^2$ and $a = 0.82226$ was computed numerically by fitting this asymptotic expression. On the other hand, the VR-VR contributions, without self-induced velocity terms, for a set of N VRs of charge m_i and position (r_i,z_i) yield [45]

$$\tilde{E}_{\text{VR-VR}} = 4\pi \sum_{\substack{i,j=1 \\ i\neq j}}^{N} m_i m_j \sqrt{r_i r_j}\, C(k_{ij}), \tag{6}$$

where

$$C(k_{ij}) = \left(\frac{2}{k_{ij}} - k_{ij}\right)\mathcal{K}(k_{ij}) - \frac{2}{k_{ij}}\mathcal{E}(k_{ij}), \tag{7}$$

$$k_{ij}^2 = \frac{4 r_i r_j}{(z_i - z_j)^2 + (r_i + r_j)^2}, \tag{8}$$

and $\mathcal{K}$ and $\mathcal{E}$ are, respectively, the complete elliptic integrals of the first and second kind and k_{ij} is their respective elliptic modulus.

Having the total energy (4), i.e., the Hamiltonian for the system of interacting VRs, we can obtain the equations of motion as a set of coupled ODEs for the vortex positions using the corresponding Hamilton's equations:

$$\dot{p}_i = -\frac{\partial E}{\partial q_i}, \qquad \dot{q}_i = \frac{\partial E}{\partial p_i}. \tag{9}$$

We follow the choice of canonical variables (p_i,q_i) from Ref. [45]:

$$(p_i,q_i) = \left(2\pi\, m_i\, r_i^2, z_i\right). \tag{10}$$

It is precisely due to this choice of canonical variables that it is not possible to apply the naïve approach of adding the resulting equations of motion from Refs. [43] and [45] as the former uses the canonical variables (10), while the latter uses $(p_i,q_i) = (r_i,z_i)$. For completeness, the resulting ODEs are included in the Appendix.

Here, it is relevant to point out some limitations of the current PP approach. First, it relies on the Hamiltonian GPE model (1) and thus is not able to capture the effects of dissipative terms due to the presence of a thermal (noncondensed) cloud and/or quantum fluctuations. It should be, in principle, possible to include phenomenological damping terms in the PP model. These damping (or, more precisely, antidamping) terms would be responsible for an antidamped oscillation of the VRs until they decay at the edge of the BEC cloud in a manner akin to the corresponding situation with point vortices in two dimensions (see, for instance, Ref. [54] and references therein). Second, our current PP is limited to coaxial VRs, which is pertinent to the VR dynamics close to the stationary states that we are interested in here. This is quite relevant, e.g., towards describing the normal modes of VR oscillations. However, this PP is not able to capture general VR interactions. In particular, as soon as the coaxiality of the VRs is violated, the PP is no longer valid. Furthermore, the PP is not able to capture scattering and/or reconnections between VRs. Possible extensions of the PP along these lines fall outside of the scope of the current paper. Nevertheless, we should note that there exists an "intermediate" level of description considering the VRs as filaments of vorticity interacting with each other via the Biot-Savart law (and the associated induced velocity field from one to the other). This is computationally less expensive than the full 3D simulation performed here, yet it is also less insightful and analytically tractable than the PP. On the other

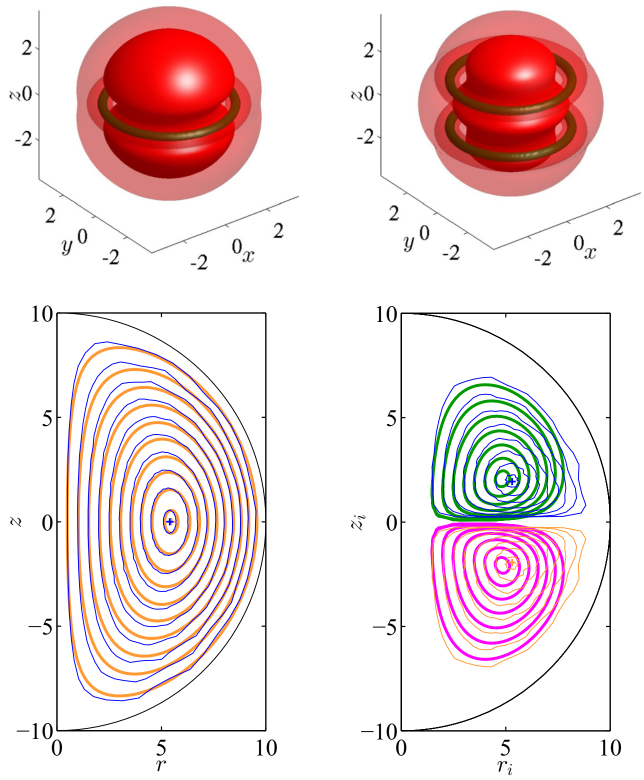

FIG. 1. The top row illustrates *stationary* single (left) and opposite-charge double (right) VRs for $\mu = 12$ in an isotropic trap with $\omega_z = \omega_r = 1$. The panels depict isocontour plots for the density (red), and the cores of the VRs are highlighted by green (dark) surfaces corresponding to isocontours of the smoothed norm of the vorticity (curl of the fluid velocity). The bottom row depicts the trajectories for one VR (left) and two oppositely charged VRs (right) in an isotropic trapping with $\omega_z = \omega_r = 1$ and $\mu = 50$. Using the cylindrical symmetry of the setup, the trajectories are depicted in the (r,z) plane, where r is the radius of the VR and z is its vertical axis coordinate. The thick solid trajectories correspond to the particle picture (PP) prediction of Sec. II B, while the thin solid trajectories correspond to numerical simulations of the GPE of Eq. (1) integrated in reduced cylindrical coordinates. The outermost semicircle corresponds to the TF radius. For full 3D numerics showing dynamic and symmetry-breaking instabilities, we refer the reader to the results in Figs. 4, 5, 7 and 8.

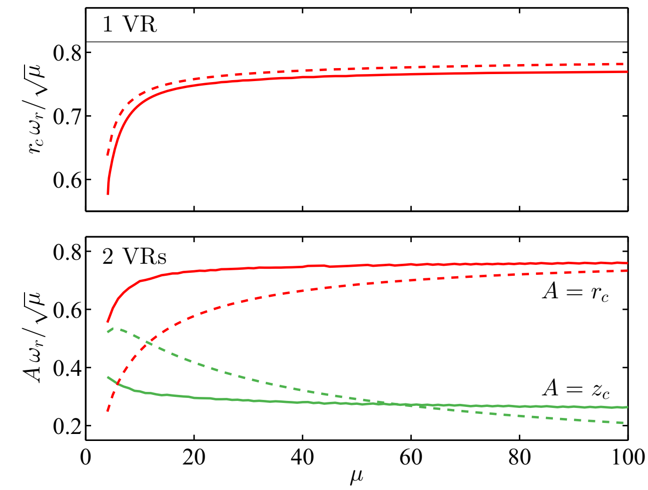

FIG. 2. Equilibrium positions for one and two opposite-charge VR configurations as a function of the chemical potential μ. The top and bottom panels show the equilibrium radius r_c and axial location z_c as a function of the dimensionless (by $\hbar\omega_r$) chemical potential μ for the particle picture (PP; dashed line) and the GPE (solid line) for the single VR (top) and double VR (bottom) for $\omega_z = \omega_r = 1$. The top panel includes (thin horizontal line) the asymptotic prediction for $\mu \to \infty$ given in Eq. (11). All quantities in this and subsequent figures are dimensionless; see text.

hand, it may handle phenomena like the bending and the loss of coaxiality of the rings [55,56]. Clearly, each approach has its own advantages and disadvantages; here, motivated by the consideration of the equilibrium and near-equilibrium settings, we will opt to consider the PP method in conjunction with full 3D numerical results.

III. RESULTS

We begin the discussion of our numerical findings by presenting existence results for the case of single and multiple VRs. The top row of panels in Fig. 1 depicts illustrative examples of the steady-state configurations for one and two opposite-charge VRs. However, if the VRs are not placed at their stationary position, they start to oscillate as depicted in the bottom row of panels in Fig. 1. These panels depict the trajectories for one VR (left panel) and two oppositely charged VRs (right panel) in an isotropic parabolic trap (2) with $\omega_r = \omega_z = 1$ and chemical potential $\mu = 50$. The thick and thin trajectories correspond, respectively, to our PP and the GPE dynamics. Figure 1 suggests that the dynamics for a single VR is qualitatively and quantitatively very well described by the PP. The case of two VRs (right panel) indicates a good qualitative match between PP and the original GPE dynamics, yet the position of the steady-state configurations seems to be slightly shifted. In order to have a broader sense of the validity of the PP, let us follow the steady-state VR positions for one and two VRs as the chemical potential is varied. Figure 2 depicts the comparison between the numerical solutions of the GPE (solid lines) and the PP (dashed lines). For a single VR (top panel), the PP does an excellent job at predicting the stationary position of the VR and its functional dependence on the chemical potential μ. Note that the $\mu \to \infty$ asymptotic prediction in the TF limit from Refs. [57,58] for the equilibrium radius r_c,

$$r_c = \sqrt{\frac{2\mu}{3\omega_r^2}}, \tag{11}$$

is slightly higher than the one predicted by the PP.

The bottom panel of Fig. 2 depicts the comparison between the GPE and PP results for the opposite-charge two-VR steady-state configuration. In this case, one can see that the trends predicted by the PP can qualitatively follow that of the full GPE, although some quantitative disparity remains. This can be attributed to the following causes:

(i) The PP is an amalgamation of different contributions stemming from different approaches; it would be useful,

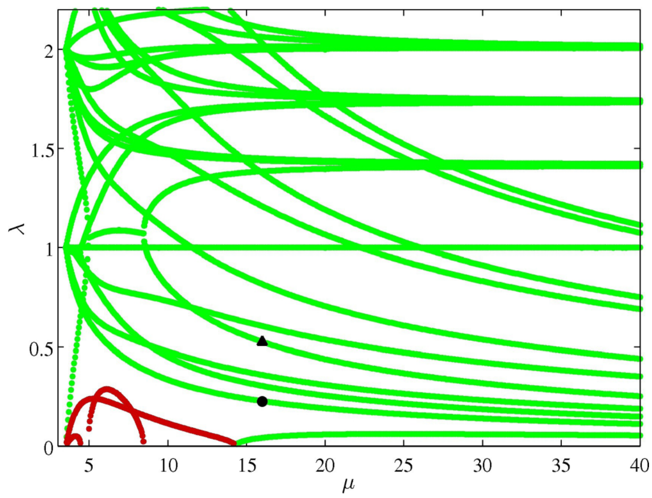

FIG. 3. BdG spectrum for two VRs as a function of the dimensionless chemical potential μ for $\omega_z = \omega_r = 1$. Mode contributions are shown via green (light) points if stable and red (dark) points if unstable. The black circle and triangle represent the frequencies for the normal-mode vibrations around the stationary state depicted, respectively, in Figs. 4 and 5.

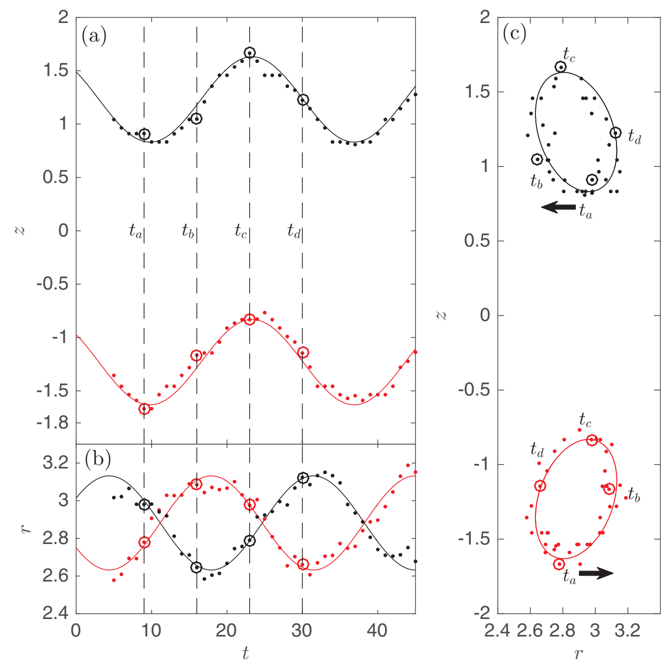

FIG. 4. The first $n = 0$ excitation of the two-VR state. Black [red (gray)] represents the upper (lower) ring. The open circles (and corresponding vertical dashed lines) indicate four time points to demonstrate the motion of the rings via their (a) time-z, (b) time-r, and (c) (r,z) trajectories. The solid curves are fits to the data, while the arrows in (c) indicate time t_a and the subsequent direction of core motion. Time and space are measured in units of $1/\omega_r$ and harmonic oscillator length $a_r = \sqrt{\hbar/m\omega_r}$, respectively.

although technically seemingly especially tedious, to consider an approach incorporating all three effects concurrently.

(ii) The accumulation of errors for the three different contributions, since each one of them involves corresponding approximations.

(iii) The interaction between the VRs is modulated by density variations, a feature that is not captured in the effective PP in the form considered herein.

This last point is also an issue that affects similar particle approaches for vortices in two dimensions and has been discussed in Refs. [59,60]. Nevertheless, we conclude that the PP approach, while less quantitatively dependable, can be used to provide a qualitative handle on the trends of stationary multi-VR characteristics.

We now turn to the exploration of the spectrum of the multi-VR states. Although a brief discussion of this can be found in Ref. [40], in the vicinity of the linear limit, here, we consider the relevant spectrum more systematically for a wide parameter range. Let us focus our attention on opposite-charge configurations with two and three VRs. The relevant spectrum for the two-VR solution is shown in Fig. 3 and is seen to bear numerous similarities to that of the single VR (discussed in Ref. [44]). In particular, the modes associated with dynamical instability are fairly similar to those of the single VR. The most significant one among them, associated with the widest parameter range of instability, is related to a quadrupolar mode having an $n = 2$ azimuthal dependence $e^{in\theta}$, as we will also see below in the dynamical-evolution results. On the other hand, the mode immediately above this one, for large μ in the spectrum, is azimuthally symmetric ($n = 0$) and is associated with a stable relative motion of the two vortex rings. The trajectory of this mode is illustrated in Fig. 4. This excitation was initiated by mixing the two-VR stationary state with the corresponding BdG excitation; the resulting wave function was then renormalized to preserve the total atom number and subsequently evolved in time according to the GPE. Since this excitation has $n = 0$, these rings have azimuthal symmetry, and the cores remain circular and coaxial with the z axis throughout the motion. In the (r,z) cross section of Fig. 4(c), the upper ring orbits clockwise while the lower ring orbits counterclockwise in such a way that their z motion remains in phase. The fitted period for this oscillation is $T = 27.1$ (in units of $1/\omega_r$), which compares favorably with the BdG prediction $T = 27.9$ (see black circle in Fig. 3). The chemical potential (in dimensionless units) was chosen as $\mu \sim 16$.

Contrary to the single VR studied in Ref. [44], the existence of an additional ring means that there is a second $n = 0$ vortex excitation. This is shown in Fig. 5 and exhibits a motion similar to that of the first excitation, but now the measured period is $T = 11.9$, compared to the BdG period of $T = 12.0$ (see black triangle in Fig. 3). Furthermore, the relative phase of the ring motion differs such that the r positions are now in phase, while the z perform an out-of-phase oscillation. Finally, the branches that level off at large μ are the nonvortex excitations of the underlying ground state.

We also provide a similar spectral perspective in the case of the opposite-charge three-VR solution in Fig. 6. The top four panels and the middle isocontour panel illustrate a characteristic example of this state for (dimensionless) chemical potential $\mu = 12$. In the cut along the central (x,y) plane, a ringlike structure is clearly discernible, while a vertical (y,z) cut reveals three pairs of opposite-charge vortices,

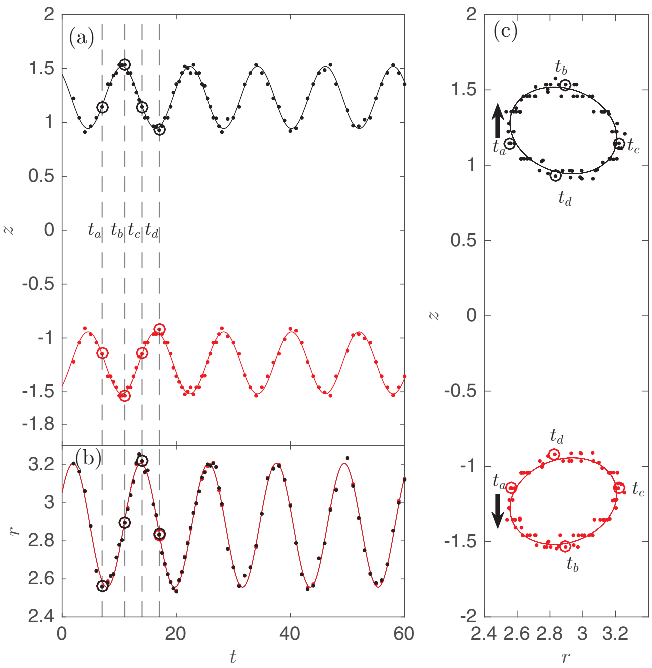

FIG. 5. The second $n = 0$ excitation of the two-vortex-ring state. Curves and labels have the same meaning as in Fig. 4. These rings, as was shown in Fig. 4 for the first excitation, have azimuthal symmetry and cores that remain circular and coaxial with the z axis throughout the motion. Note that in (b) the r motions of the two rings are in phase and the data points overlap. As explained in the caption of Fig. 4, $\mu \sim 16$. Time and space are measured in units of $1/\omega_r$ and harmonic oscillator length $a_r = \sqrt{\hbar/m\omega_r}$.

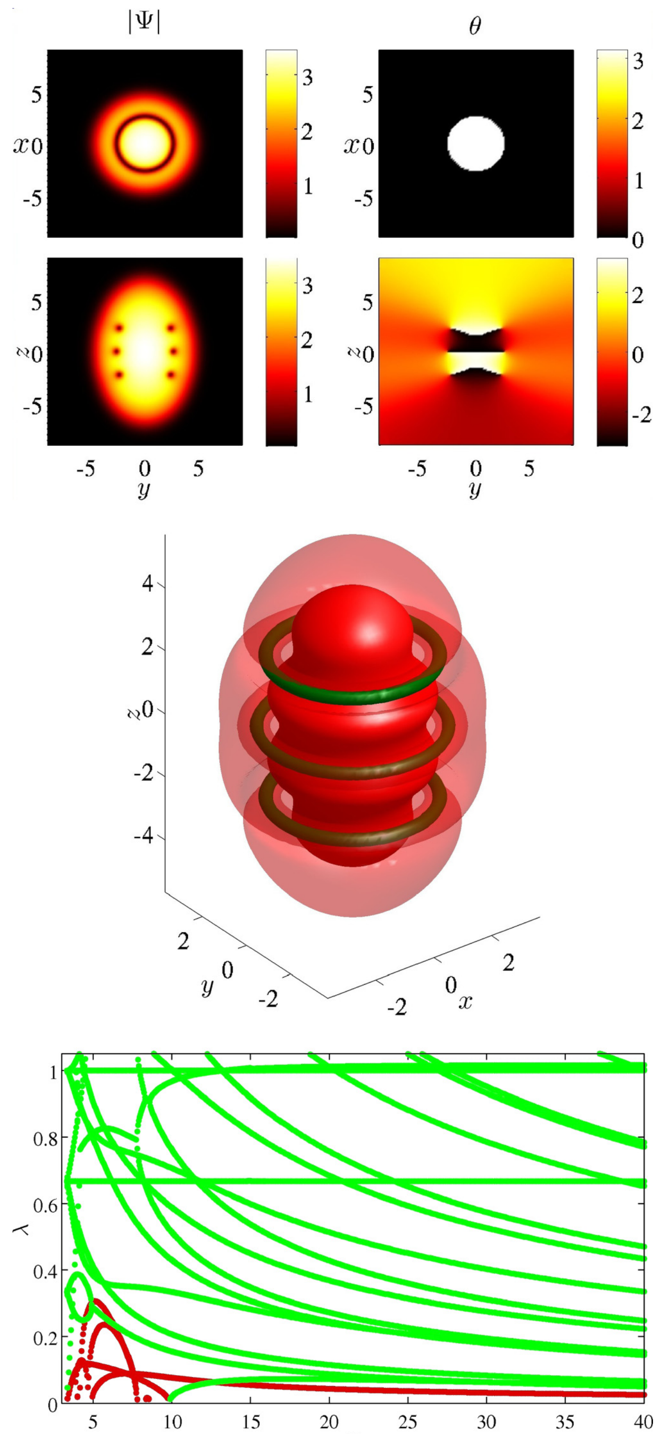

FIG. 6. The opposite-charge three-VR configuration for $\frac{3}{2}\omega_z = \omega_r = 1$. The top four panels show the modulus $|\Psi|$ (left) and argument θ (right) of a triple-vortex-ring state for a dimensionless chemical potential $\mu = 12$; the first row illustrates the $z = 0$ plane, while the second row illustrates the $x = 0$ plane. The middle panel shows an isocontour density plot. The bottom panel depicts the BdG spectrum for the three-VR configuration as a function of the dimensionless chemical potential μ. Notation is the same as in Fig. 3. Notice the higher multiplicity of unstable modes and especially the persistent, albeit weakening, instability due to an eigenmode resulting from the collision of two modes around $\mu = 5$.

alternating along the y axis, as well as along the z axis. This implies that the three rings, given the alternating nature of the constituent triple-soliton pattern, result in an equilibrium triplet of vortex rings of charge $+1$, -1, and $+1$, up to parity reversals of all three. The middle panel clearly showcases, through its density isocontours, the nature of the pattern. The bottom panel in Fig. 6 depicts the BdG spectrum for the three-VR solution as the chemical potential is varied. While some of the oscillatory instabilities associated with complex eigenvalues appear over narrow parameter intervals, for small values of $\mu < 10$, there is an instability arising from the collision of two eigenmodes near $\mu = 5$ that seems to persist for $\mu > 10$ and indeed for the entire parametric interval of chemical potentials that we have explored. We will explore this dynamical mode in the direct numerical simulations that follow, as it seems the most pertinent one to the potential stability of multi-VR states in the TF regime of large μ. We note that this instability might be *suppressed* by adjusting the trap aspect ratio. This was indeed the case for single-vortex rings, where they are predicted to be stable for mildly oblate trapping potentials $1 \leqslant \omega_z/\omega_r \leqslant 2$ [43,44]. Again, we have checked that the modes that level off are bulk excitations of the underlying ground state.

We now explore some of the key dynamical features of multi-VRs through direct numerical simulations. In Fig. 7, we examine a rather intriguing example of the dynamical

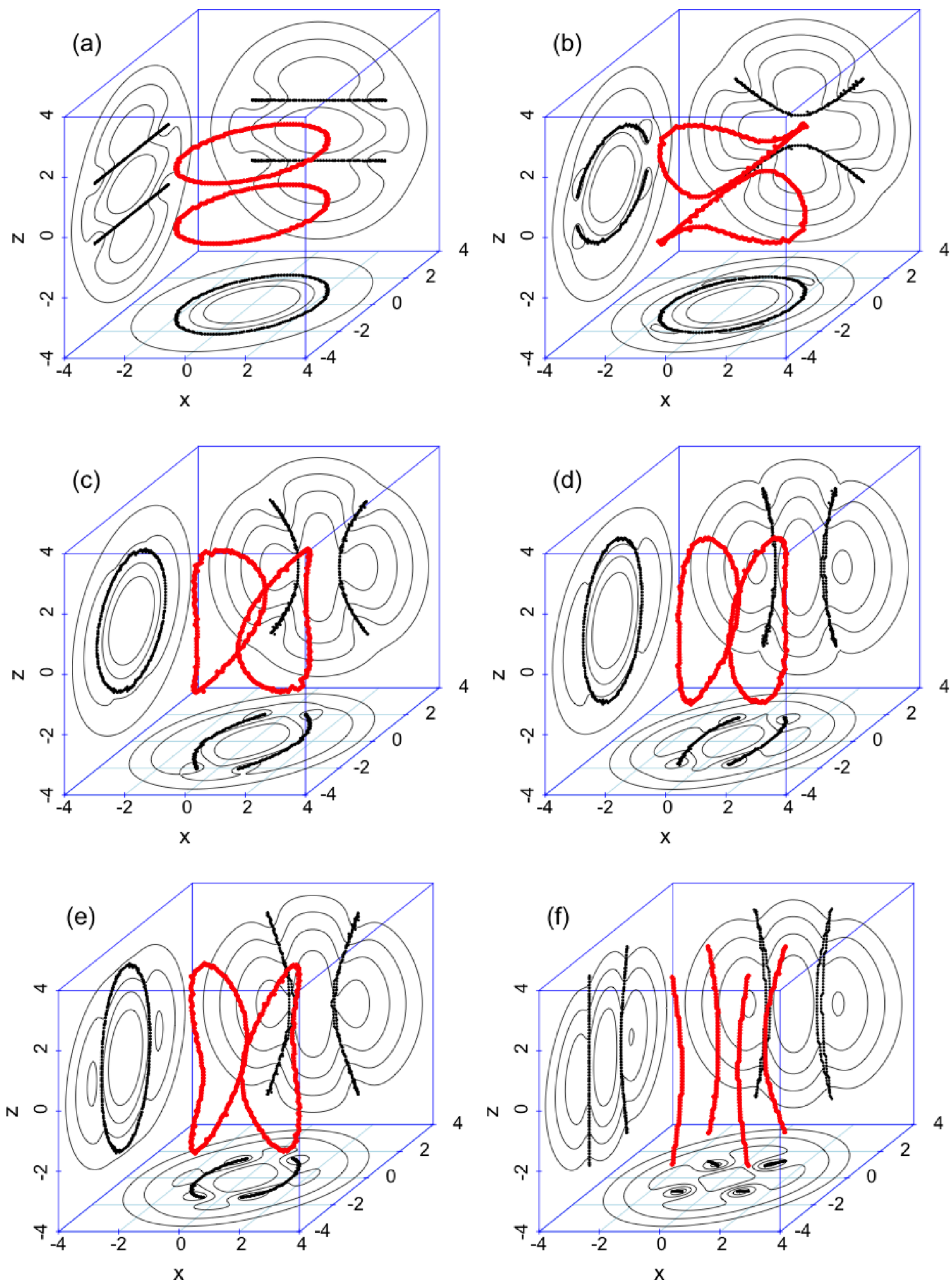

FIG. 7. Evolution of an unstable double-vortex ring for chemical potential $\mu = 10$. Six representative snapshots during the time evolution of the state are given at times $t =$ (a) 20, (b) 40, (c) 45.4, (d) 68, (e) 71.2, and (f) 74.8 (units of $1/\omega_r$). Notice the intense quadrupolar undulation of the rings leading to their breakup and then reconnection with a perpendicular axis of symmetry, as well as an example of their breakup into vortex lines along the z direction.

instability of the two-VR state for $\mu = 10$. In this figure we show the 3D positions of the vortex core as red curves [61], and their projections onto the (x,y), (x,z), and (y,z) planes are shown as black curves. Two-dimensional density contours are also projected on these three planes, and the contours correspond to 0.25, 0.5, and 0.75 of the maximum density at each time. We observe that the rings initially deform in a quadrupolar fashion, and once this deformation becomes sufficiently severe, they split and reconnect as (nearly) coaxial rings perpendicular to their original orientation. The rotated double rings remain robust for a considerable time interval, as can be seen in Figs. 7(c)–7(e), which span $\Delta t \sim 25$. We have also observed that, depending on the initial conditions, two VRs can undergo this effective rotation several times, sometimes transiently breaking into four vortex lines, as shown in Fig. 7(f), before reforming as a rotated double VR. Eventually, however, the VRs break up into a vortex tangle, and the time scale over which this occurs depends on the initial

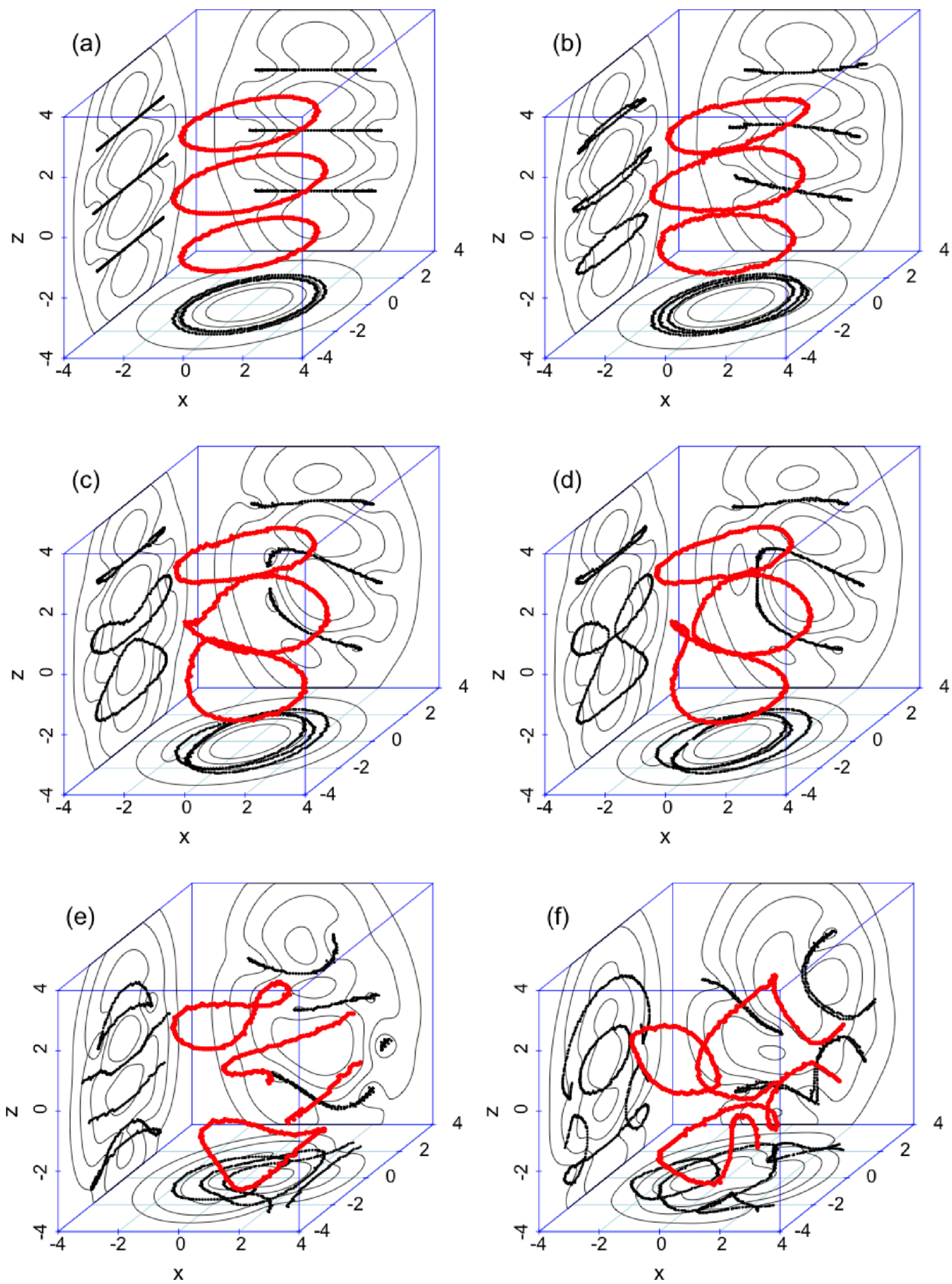

FIG. 8. As in Fig. 7 but for the unstable evolution of the three-vortex-ring state in the case of $\mu = 9$. The six representative snapshots shown during the time evolution correspond in this case to $t =$ (a) 20, (b) 49.4, (c) 52.4, (d) 53.3, (e) 54.9, and (f) 56.0 (units of $1/\omega_r$). Notice how the deformation of the rings leads, in this case, to the joining of the two lower ones into a single entity [see (d)] before the subsequent evolution to a vortex tangle.

conditions. Furthermore, small-amplitude perturbations break the symmetry of the resulting evolution, inhibiting the full recurrence back to the original configuration.

Last, we examine a prototypical example of the instability associated with the three-VR state. We probe, in particular, the unstable mode that was observed in Fig. 6 to be the persistent cause of instability for large values of the chemical potential. This instability in the case of $\mu = 9$ is illustrated in Fig. 8. There, it can be observed that the triple VR becomes subject to a symmetry-breaking deformation of the rings. As time evolves, the resulting undulations are amplified and lead to intense Kelvin-mode excitations along each of the rings. Subsequently, two of these rings may combine, as can be seen in Fig. 8(d). These two rings then separate again, as shown in Fig. 8(e), and eventually, all three rings again evolve into a vortex tangle, as shown in Fig. 8(f).

IV. DISCUSSION AND FUTURE CHALLENGES

In the present work, we have extended the analytical and numerical examination concerning the dynamics of single and multiple VRs in harmonically confined Bose-Einstein condensates. We showed that in such systems it is controllably possible to form and establish the existence of states involving one, two, three, or more VRs essentially at will over a wide range of chemical potentials, or, equivalently, atom numbers. Furthermore, we provided a theoretical formulation based on the energetics of the different processes involving the rings at the particle level. We demonstrated that for the one-, two-, and three-VR states considered herein this approach, encompassing the self-induced ring translation, the trap-induced ring oscillation, and the inter-ring interaction, could capture qualitatively and in some cases quantitatively the ring steady states. The stability of these multi-VR steady states was also probed at the level of a full Bogoliubov–de Gennes analysis which revealed both the instabilities of, e.g., two- and three-VR states and also the collective relative motions of the rings. Finally, some selected examples of the dynamics of the VRs were displayed, demonstrating both their potential for coherent multi-VR motions and also their rich instability scenarios containing examples of VR breakups and recombinations. Such events include ring mergers and subsequent splits or redistribution of the vorticity in the form of vortex lines.

There are numerous questions that remain open and constitute interesting directions for future work. First, for single or multiple vortex rings, identifying an approach, perhaps involving an adiabatic invariant as in Refs. [62–65], that would give a more accurate description of its equilibrium and overall dynamics would be helpful both in the realm of a single VR and in that of multiple VRs.

Second, it would be interesting, albeit technically demanding, to attempt to incorporate the density modulations in the inter-ring interactions in a way similar to what was proposed for ordinary vortices in Ref. [59]. A perhaps more straightforward, although computationally demanding possibility, would be to explore the dynamics of VRs in a way similar to that of Ref. [55]. In that work, the authors used the full Biot-Savart law in order to explore the interactions between numerous initially coaxial vortex rings in a uniform medium with the aim of studying their leapfrogging behavior. The Biot-Savart law encompasses two out of the three features we are considering here, namely, the ring self-action and the inter-ring interaction. It does not include the effect of the trap, yet this can be accounted for through the work of Ref. [42]. The combination of these approaches would then enable at an effective, rather than full GPE, level the examination of not solely coaxial vortex rings as is done here but also their deformation (beyond coaxiality) while considering their motion. Comparing such a sophisticated approach with the full Gross-Pitaevskii dynamics would be especially informative.

Naturally, also, extensions of the present considerations to a higher number of components, including the potential formation of more exotic structural configurations such as Skyrmions [66,67], would be of interest as well for future work.

Progress along some of these directions, when relevant, will be reported in future publications.

ACKNOWLEDGMENTS

W.W. acknowledges support from NSF Grant No. DMR-1151387 and from the Office of the Director of National Intelligence (ODNI), Intelligence Advance Research Projects Activity (IARPA), via MIT Lincoln Laboratory Air Force Contract No. FA8721-05-C-0002. R.N.B. is supported by the QUIC grant of the Horizon 2020 FET program and by Provincia Autonoma di Trento. R.N.B., C.T., L.A.C., and P.G.K. acknowledge support from Los Alamos National Laboratory, which is operated by LANS, LLC for the NNSA of the U.S. DOE and, specifically, Contract No. DEAC52-06NA25396. R.C.-G. gratefully acknowledges the support of NSF Grants No. DMS-1309035 and No. PHY-1603058. P.G.K. gratefully acknowledges the support from NSF Grants No. DMS-1312856 and No. PHY-1602994, from the ERC under FP7, Marie Curie Actions, People, International Research Staff Exchange Scheme (IRSES-605096), and from the Stavros Niarchos Foundation via the Greek Diaspora Fellowship Program. We thank the Texas A&M University for access to their Ada cluster.

APPENDIX: EFFECTIVE ODEs FOR TRAPPED VRs

Here, we include the explicit effective ODEs describing the dynamics of N VRs with radii r_i and vertical positions z_i inside an isotropic trap with strength ω and TF radius $R_\perp = \sqrt{2\mu}/\omega$ for chemical potential μ. By using Hamilton's equations (9), the dynamics for each VR is given by

$$\dot{r}_i = \dot{r}_i^{\text{(VR-T)}} + \dot{r}_i^{\text{(VR-VR)}},$$
$$\dot{z}_i = \dot{z}_i^{\text{(VR-T)}} + \dot{z}_i^{\text{(VR-VR)}},$$

where the contributions due to the trap are encapsulated in the VR-T terms and the vortex-vortex interactions are encapsulated in the VR-VR terms. The VR-T contributions yield

$$\dot{r}_i^{\text{(VR-T)}} = 2\alpha\, r_i z_i (L-1),$$
$$\dot{z}_i^{\text{(VR-T)}} = \alpha\left(R_\perp^2 - 3\,r_i^2 - z_i^2\right)L - 2\alpha\left(R_\perp^2 - 2\,r_i^2 - z_i^2\right),$$

where

$$L = \ln\left(\frac{R_\perp^2 - \left(r_i^2 + z_i^2\right)}{\xi^2}\right),$$

$$\alpha = \frac{\pi^2\mu}{2r_i R_\perp^2}.$$

On the other hand, the VR-VR contributions yield

$$\dot{r}_i^{(\text{VR-VR})} = -\frac{1}{m_i r_i}\sum_{j\neq i}^{N}\frac{\partial W_{ij}}{\partial z_i},$$

$$\dot{z}_i^{(\text{VR-VR})} = +\frac{1}{m_i r_i}\sum_{j\neq i}^{N}\frac{\partial W_{ij}}{\partial r_i},$$

where

$$W_{ij} = m_i m_j \sqrt{r_i r_j}\, C(k_{ij})$$

and $C(k_{ij})$ is defined in Eq. (7).

[1] C. J. Pethick and H. Smith, *Bose-Einstein Condensation in Dilute Gases* (Cambridge University Press, Cambridge, 2008).
[2] L. P. Pitaevskii and S. Stringari, *Bose-Einstein Condensation* (Oxford University Press, Oxford, 2003).
[3] V. S. Bagnato, D. J. Frantzeskakis, P. G. Kevrekidis, B. A. Malomed, and D. Mihalache, Rom. Rep. Phys. **67**, 5 (2015).
[4] D. Mihalache, Rom. J. Phys. **59**, 295 (2014).
[5] *Emergent Nonlinear Phenomena in Bose-Einstein Condensates: Theory and Experiment*, edited by P. G. Kevrekidis, D. J. Frantzeskakis, and R. Carretero-González (Springer, Berlin, 2008); R. Carretero-González, D. J. Frantzeskakis, and P. G. Kevrekidis, Nonlinearity **21**, R139 (2008).
[6] P. G. Kevrekidis, D. J. Frantzeskakis, and R. Carretero-González, *The Defocusing Nonlinear Schrödinger Equation: From Dark Solitons to Vortices and Vortex Rings* (Society for Industrial and Applied Mathematics, Philadelphia, 2015).
[7] M. J. Ablowitz and H. Segur, *Solitons and the Inverse Scattering Transform* (Society for Industrial and Applied Mathematics, Philadelphia, 1981).
[8] M. J. Ablowitz and P. A. Clarkson, *Solitons, Nonlinear Evolution Equations and Inverse Scattering* (Cambridge University Press, Cambridge, 1991).
[9] M. J. Ablowitz, B. Prinari, and A. D. Trubatch, *Discrete and Continuous Nonlinear Schrödinger Systems* (Cambridge University Press, Cambridge, 2004).
[10] C. Sulem and P. L. Sulem, *The Nonlinear Schrödinger Equation* (Springer, New York, 1999).
[11] K. E. Strecker, G. B. Partridge, A. G. Truscott, and R. G. Hulet, Nature (London) **417**, 150 (2002).
[12] L. Khaykovich, F. Schreck, G. Ferrari, T. Bourdel, J. Cubizolles, L. D. Carr, Y. Castin, and C. Salomon, Science **296**, 1290 (2002).
[13] S. L. Cornish, S. T. Thompson, and C. E. Wieman, Phys. Rev. Lett. **96**, 170401 (2006).
[14] O. Morsch and M. Oberthaler, Rev. Mod. Phys. **78**, 179 (2006).
[15] D. J. Frantzeskakis, J. Phys. A **43**, 213001 (2010).
[16] A. L. Fetter and A. A. Svidzinsky, J. Phys. Condens. Matter **13**, R135 (2001).
[17] A. L. Fetter, Rev. Mod. Phys. **81**, 647 (2009).
[18] S. Komineas, Eur. Phys. J. Spec. Top. **147**, 133 (2007).
[19] J. Koplik and H. Levine, Phys. Rev. Lett. **76**, 4745 (1996).
[20] P. G. Saffman, *Vortex Dynamics* (Cambridge University Press, Cambridge, 1992).
[21] L. M. Pismen, *Vortices in Nonlinear Fields* (Clarendon, Oxford, 1999).
[22] R. J. Donnelly, *Quantized Vortices in Helium II* (Cambridge University Press, Cambridge, 1991).
[23] G. W. Rayfield and F. Reif, Phys. Rev. **136**, A1194 (1964).
[24] G. Gamota, Phys. Rev. Lett. **31**, 517 (1973).
[25] B. P. Anderson, P. C. Haljan, C. A. Regal, D. L. Feder, L. A. Collins, C. W. Clark, and E. A. Cornell, Phys. Rev. Lett. **86**, 2926 (2001).
[26] I. Shomroni, E. Lahoud, S. Levy, and J. Steinhauer, Nat. Phys. **5**, 193 (2009).
[27] N. S. Ginsberg, J. Brand, and L. V. Hau, Phys. Rev. Lett. **94**, 040403 (2005).
[28] C. Becker, K. Sengstock, P. Schmelcher, P. G. Kevrekidis, and R. Carretero-González, New J. Phys. **15**, 113028 (2013).
[29] M. C. Tsatsos, P. E. S. Tavares, A. Cidrim, A. R. Fritsch, M. A. Caracanhas, F. Ednilson, A. dos Santos, C. Barenghi, and V. S. Bagnato, Phys. Rep. **622**, 1 (2016).
[30] N. Navon, A. L. Gaunt, R. P. Smith, and Z. Hadzibabic, Nature (London) **539**, 72 (2016).
[31] M. T. Reeves, T. P. Billam, B. P. Anderson, and A. S. Bradley, Phys. Rev. Lett. **114**, 155302 (2015).
[32] P. Clark di Leoni, P. D. Mininni, and M. E. Brachet, Phys. Rev. A **94**, 043605 (2016).
[33] M. W. Scheeler, D. Kleckner, D. Proment, G. L. Kindlmann, and W. T. M. Irvine, Proc. Natl. Acad. Sci. USA **111**, 15350 (2014).
[34] D. Kleckner, L. H. Kauffman, and W. T. M. Irvine, Nat. Phys. **12**, 650 (2016)
[35] E. Kozik and B. Svistunov, Phys. Rev. Lett. **92**, 035301 (2004).
[36] E. Kozik and B. Svistunov, Phys. Rev. Lett. **94**, 025301 (2005).
[37] M. Leadbeater, T. Winiecki, D. C. Samuels, C. F. Barenghi, and C. S. Adams, Phys. Rev. Lett. **86**, 1410 (2001).
[38] I. Bloch, J. Dalibard, and W. Zwerger, Rev. Mod. Phys. **80**, 885 (2008); *Quantum Gases: Finite Temperature and Non-equilibrium Dynamics*, edited by N. Proukakis, S. Gardiner, M. Davis, and M. Szymańska (Imperial College Press, London, 2013).
[39] L.-C. Crasovan, V. M. Pérez-García, I. Danaila, D. Mihalache, and L. Torner, Phys. Rev. A **70**, 033605 (2004).
[40] R. N. Bisset, W. Wang, C. Ticknor, R. Carretero-González, D. J. Frantzeskakis, L. A. Collins, and P. G. Kevrekidis, Phys. Rev. A **92**, 043601 (2015).
[41] B. Jackson, J. F. McCann, and C. S. Adams, Phys. Rev. A **60**, 4882 (1999).
[42] A. A. Svidzinsky and A. L. Fetter, Phys. Rev. A **62**, 063617 (2000).
[43] T.-L. Horng, S.-C. Gou, and T.-C. Lin, Phys. Rev. A **74**, 041603 (2006).
[44] R. N. Bisset, W. Wang, C. Ticknor, R. Carretero-González, D. J. Frantzeskakis, L. A. Collins, and P. G. Kevrekidis, Phys. Rev. A **92**, 063611 (2015).
[45] M. Konstantinov, Phys. Fluids **6**, 1752 (1994).

[46] B. N. Shashikanth and J. E. Marsden, Fluid Dyn. Res. **33**, 333 (2003).

[47] R. M. Caplan, J. D. Talley, R. Carretero-González, and P. G. Kevrekidis, Phys. Fluids **26**, 097101 (2014).

[48] B. I. Schneider, L. A. Collins, and S. X. Hu, Phys. Rev. E **73**, 036708 (2006).

[49] As an example, for the GPE solution of the two-vortex ring spherical case with a chemical potential of $\sim 16\hbar\omega_r$ and $4\pi N a_s \sqrt{m\omega_r/\hbar} = 4413$, we employ in each Cartesian coordinate a grid of 257 points derived from 64 elements with an order-5 Gauss-Legendre quadrature, spanning a range of $[-8.2,8.2]$ trap units, with a time step of 1.0×10^{-4}.

[50] S. Ronen, D. C. E. Bortolotti, and J. L. Bohn, Phys. Rev. A **74**, 013623 (2006).

[51] P. B. Blakie, D. Baillie, and R. N. Bisset, Phys. Rev. A **86**, 021604(R) (2012).

[52] P. H. Roberts and J. Grant, J. Phys. A **4**, 55 (1971).

[53] B. Jackson, J. F. McCann, and C. S. Adams, Phys. Rev. A **61**, 013604 (1999).

[54] D. Yan, R. Carretero-González, D. J. Frantzeskakis, P. G. Kevrekidis, N. P. Proukakis, and D. Spirn, Phys. Rev. A **89**, 043613 (2014).

[55] D. H. Wacks, A. W. Baggaley, and C. F. Barenghi, Phys. Fluids **26**, 027102 (2014).

[56] D. H. Wacks, A. W. Baggaley, and C. F. Barenghi, Phys. Rev. B **90**, 224514 (2014).

[57] W. Wang, P. G. Kevrekidis, R. Carretero-González, D. J. Frantzeskakis, T. J. Kaper, and M. Ma, Phys. Rev. A **92**, 033611 (2015).

[58] W. Wang, P. G. Kevrekidis, R. Carretero-González, and D. J. Frantzeskakis, Phys. Rev. A **93**, 023630 (2016).

[59] S. McEndoo and Th. Busch, Phys. Rev. A **79**, 053616 (2009).

[60] S. Middelkamp, P. G. Kevrekidis, D. J. Frantzeskakis, R. Carretero-González, and P. Schmelcher, Phys. Rev. A **82**, 013646 (2010).

[61] C. J. Foster, P. B. Blakie, and M. J. Davis, Phys. Rev. A **81**, 023623 (2010).

[62] Th. Busch and J. R. Anglin, Phys. Rev. Lett. **87**, 010401 (2001).

[63] V. V. Konotop and L. Pitaevskii, Phys. Rev. Lett. **93**, 240403 (2004).

[64] A. M. Kamchatnov and S. V. Korneev, Phys. Lett. A **374**, 4625 (2010).

[65] P. G. Kevrekidis, W. Wang, R. Carretero-González, and D. J. Frantzeskakis, arXiv:1701.04959.

[66] J. Ruostekoski and J. R. Anglin, Phys. Rev. Lett. **86**, 3934 (2001).

[67] C. M. Savage and J. Ruostekoski, Phys. Rev. Lett. **91**, 010403 (2003).